IEEE Access
Multidisciplinary | Rapid Review | Open Access Journal

Received June 24, 2019, accepted August 1, 2019, date of publication August 8, 2019, date of current version August 23, 2019.

Digital Object Identifier 10.1109/ACCESS.2019.2933949

A Three-Phase to Single-Phase AC-DC-AC Topology Based on Multi-Converter in AC Electric Railway Application

LINWEI LI, MINGLI WU, SI WU, JING LI, AND KEJIAN SONG
School of Electrical Engineering, Traction Power Supply Institute, Beijing Jiaotong University, Beijing 100044, China

Corresponding author: Mingli Wu (mlwu@bjtu.edu.cn)

This work was supported in part by the Fundamental Research Funds for the Central Universities under Grant 2018JBZ101, and in part by the National Postdoctoral Program for Innovative Talents under Project BX201700026.

ABSTRACT An AC-DC-AC topology based on multi-converter is proposed in this paper. It can match the capacity of the converter for high voltage and large power applications. This structure is not only suitable for solving the power quality problems of electrified railways, but also has its own superiorities. Its architecture and advantages in the traction application are analyzed in depth, and the design calculation of the main elements is presented. The control system of the proposed topology is designed, where dc current feedforward control is adopted to relieve the impact of the load mutation on the system. Its modular structure and simple current sharing control provide convenience for the capacity expansion. The software simulation and experiment based on a 45kVA prototype validate the proposed structure, and they are all compared with the traditional power supply systems. The simulation results indicate that this topology can not only satisfy the voltage and power requirements of traction load and solve the power quality problems, but also have its own superiorities in the application of electrified railways. The experimental results verify the correctness and validity of the scheme.

INDEX TERMS Electrified railways, power quality, series-parallel structure, back-to-back converter, current sharing control.

I. INTRODUCTION

In traditional traction power supply systems (TPSSs) that adopt split catenaries [1], there exist power quality problems, such as negative sequence current, harmonics and reactive power [2], [3]. As locomotives based on Pulse-Width-Modulation (PWM) are widely used, the problems of harmonics and reactive power have been improved partially [4], [5], but the problem of negative sequence current is still critical because loads on two feeders of the substation are seldom balanced due to the variable number, speed, and location of locomotives, and the capacity of the transformer is not fully utilized in this condition. Moreover, neutral sections [6], [7] inserted result in speed restriction and the loss of traction force, and the energy utilization is reduced. With the development of high-speed railway, negative sequence current and neutral section become two major problems to be solved.

Aiming at the problems of power quality and neutral section, a variety of solutions were employed. For example, passive compensation technology represented by static var compensator (SVC) [8], [9] and active compensation technology, such as static synchronous compensator (STATCOM) [10], [11] and active power filter (APF) [12], [13], were adopted in public grid or traction network to deal with these problems. The railway static power condition (RPC) [14]–[17] employed in Japan can solve the power quality problems of electrified railways, especially negative sequence current. However, the above solutions only focus on some aspects of these power quality problems. SVC, STATCOM and APF are mainly used to solve the problems of reactive power and harmonics, while RPC mainly deals

The associate editor coordinating the review of this article and approving it for publication was Ton Do.

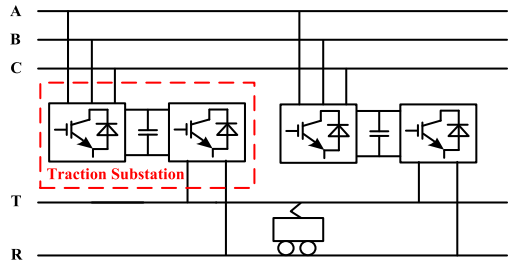

FIGURE 1. The schematic diagram of the power electronics converter-based scheme.

with the problem of negative sequence current. Therefore, the above methods do not solve the power quality problems in electrified railways thoroughly, and neutral sections can not be removed.

In order to solve the power quality problems and neutral sections thoroughly, three-phase to single-phase power conversion should be adopted in the traction substation. There are two main schemes at present. The first one is the compensator-based scheme. The equipment based on active power compensator (APC) designed by Chinese scholars, which is called co-phase traction power supply system, is analyzed in [18], [19]. The APC can balance active power between two secondary windings of the transformer, and compensate reactive power and harmonics of the load. However, the magnitude, phase and frequency of the output voltage can not be controlled, so neutral sections can only be halved.

The second one is the power electronics converter-based scheme, presented in Fig.1. It refers to the German traction power supply mode [1]. Three-phase ac power can be converted directly to single-phase ac power required by traction load in traction substation. Owing to the flexible control, this scheme is a better choice compared with the compensator-based solution. It can not only solve the power quality problems at the point of common coupling (PCC), but also remove all neutral sections. Furthermore, this system can also compensate reactive power and harmonics of the train.

In this solution, the main circuit of the traction substation was studied by some scholars and engineers. The high voltage and high power characteristics of traction power supply systems indicate that the traditional single two-level or tri-level converter [20] can not meet the requirements. Recently, with the development of power electronic technology, the appearance of multi-level structure promotes the power electronic converter application in the high voltage and large capacity field. In Datteln, west Germany, the world's largest railway power supply converter station was established based on diode clamped multilevel converter (DCMC) [21]. This system adopts standardized module to facilitate maintenance, but also has some defects. There is a three-phase transformer at the input side and a low-frequency transformer at the output side. The loss and cost of these transformers occupy a large proportion of the total cost, and the noise problem is also serious. To solve this problem, a topology without single-phase low frequency transformer based on Neutral-Point-Clamped (NPC) was proposed in [22]. It reduces the cost and improves the efficiency, but it is not suitable for the TPSSs in China because the amplitude and frequency of the voltage of the traction network are different from the Germany ones. The NPC-based structures were proposed by some Chinese scholars in [23], [24]. In these topology, with the increase of the levels, the switching devices increase sharply. Moreover, in the active power conversion process, the unbalanced dc voltage will poses a challenge to the switch devices. In addition, it has neutral potential drift problem. In order to solve the problems of the severe voltage drop caused by dense train schedule in the Tokaido Shinkansen, the power transmission equipment electronic frequency converter (EFC) based on three-phase AC to single-phase AC power conversion was equipped in the traction network in Japan [25], [26]. It has the ability to solve the problem of neutral section, but this function is not applied in practice. This structure obtains the simple voltage control, but has too many transformers. Modular multilevel converter (MMC)-based structures were proposed to apply in the traction substation in [27], [28]. MMC structure, however, requires more modules in order to achieve a specific level, which results in more capacitances and signal acquisition equipments, and circulating current suppression also makes the control system more complex [29]–[32]. Therefore, it is only verified on the low-power platform, and there is still some distance left before traction applications.

In this paper, an ac-dc-ac topology based on multi-converter is presented. The multiple structure is adopted at the input side, and the output side uses the cascade-parallel structure. It can solve the problems of the power quality in the electrified railways, and remove all neutral sections owing to the controllable output voltage. Moreover, it has its own superiorities compared with the traction converter station topologies proposed by predecessors:

1) The three-phase symmetrical and decoupled structure is more suitable for solving the negative sequence current problem of electrified railways.

2) The cascade-parallel structure at the output side allows the switching devices with low voltage and low current stress to obtain the high output voltage and large output current. The capacity expansion is easy and the loss is reduced. In addition, the design of active front end (AFE) improves the voltage sharing performance of dc-links among modules.

3) The PWM-based H-bridge adopted in the back-to-back module does not have neutral potential drift problem and it is easy to control.

Based on the above characteristics, it is more capable of traction applications.

This paper is organized as follows. Section **II** presents the architecture and analyzes the topology and its advantages applied in electrified railways in depth. The control system is described in Section **III**. The simulation and experimental results are displayed in Section **IV**. Finally, the conclusion is given in Section **V.**

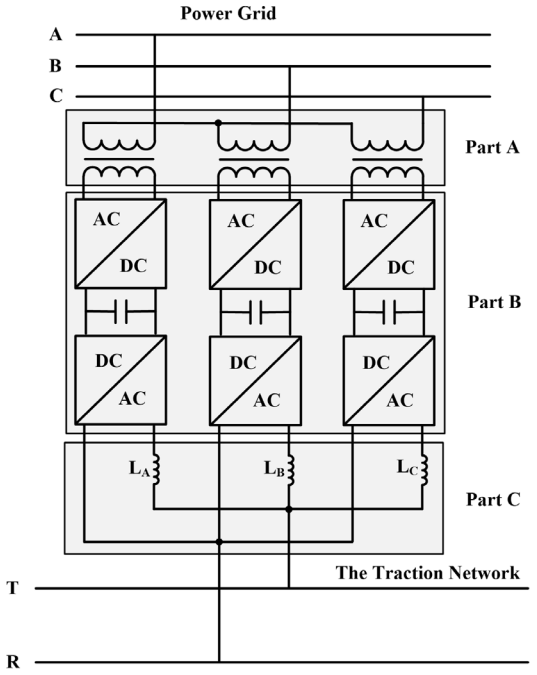

FIGURE 2. The schematic diagram of the proposed topology.

II. SYSTEM ARCHTECTURE

A. THE OVERALL STRUCTURE

The structure of the proposed topology is shown in Fig. 2. It transmits power from public grid to traction network based on three-phase to single-phase ac-dc-ac power conversion. It consists of three parts:

1) PART A

Traction substations usually draw electricity from public grid, so the transformer is needed to match the high voltage occassion. In this structure, three single-phase transformers are adopted. The primary sides of the single-phase transformers are connected in Y-type. This makes the control and structure decouple among three phases. The voltage of the secondary winding is associated with dc voltage. The calculation of the transformer capacity is described in the following section.

2) PART B

AC-DC-AC converter is the main power conversion part. Pulse-Width-Modulation (PWM)-based power electronic devices are employed to achieve power and voltage control. The converters transmit power from the utility grid to the load. AC-DC-AC structure decouples the control of the rectifier and the inverter, so the rectifier and the inverter can be controlled independently. Rectifier converts the ac power to dc power, and control the source current and dc voltage. Unity power factor operation and bidirectional power flow can be achieved, so they improve the power quality of PCC and energy utilization. Inverter converts the dc power to ac power, and control the output voltage. All neutral sections can be removed due to the controllable output voltage.

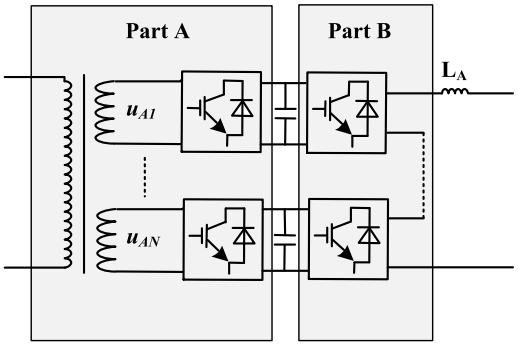

FIGURE 3. The schematic diagram of the single phase.

3) PART C

The output side of the system is connected in parallel. In this way, the switching devices with low current stress can be used to obtain large output current, so the cost is saved. For the parallel structure, we should adopt the appropriate control algorithm on the circulating current suppression.

The series inductances inserted at the output have two main effects, which include:

1) Decouple the voltage the traction network and the output voltage of the equipment, and meet the load active and reactive power requirements.

2) Smooth the output voltage and reduce the harmonic content.

Besides, the inductance also has the ability to suppress the circulating current. The selection of the inductance is important, which will be presented in the design calculation part of the elements.

B. THE AYALYSIS FOR THE SINGLE PHASE

Because of three-phase symmetric structure, we only study one phase. The schematic diagram of the single-phase structure where phase-A is taken as an example is presented in Fig.3. It includes two main parts: multiple structure and cascade structure.

1) PART A

Due to the leakage resistance of the transformer, the source voltage of the secondary windings will contain a lot of harmonics. Combine multiple structure and phase-shift sinusoidal pulse-width modulation (PS-SPWM), the harmonic content of the source current at the PCC will be reduced greatly [33]. Each secondary winding is independent on the aspect of structure, so the control is simple because we just need to control the single-phase PWM rectifier.

2) PART B

In order to obtain the high voltage to the traction application, cascade converters are adopted. More levels could be acquired with the modules increasing in this structure. Meanwhile, the capacity can also be expanded. Moreover, high modularity makes maintenance more convenient and it also supports redundancy. These advantages provide convenience for electrified railway application.

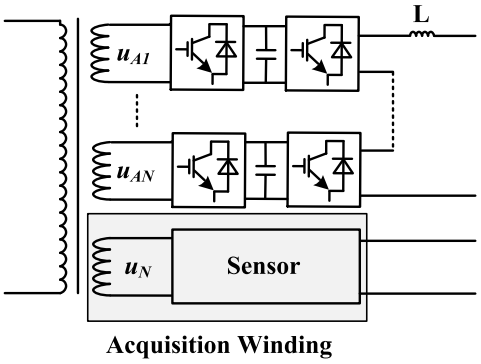

FIGURE 4. The schematic diagram of the single phase with acquisition winding.

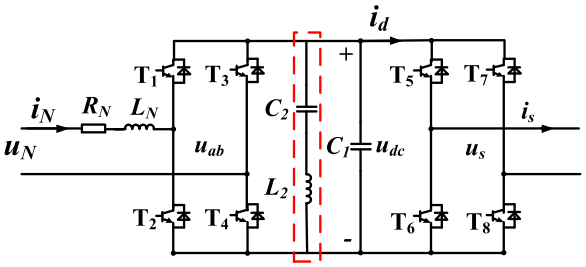

FIGURE 5. The schematic diagram of the back-to-back converter.

C. ACQUISITION FOR THE SINGLE-PHASE PWM RECTIFIER

If the ac voltage signal of each single-phase PWM rectifier is acquired separately, the following drawbacks will be caused:

(1) Although each secondary winding of the multi-winding transformer is uniform in theory on the hardware configuration, there is always be different in practical application due to various reasons. So, the ac voltage single acquired of each rectifier will not be the same, even quite different. This will increase the unbalance degree of dc voltage and the harmonic content of source current in the primary side.

(2) Too many acquisition devices will result in a large size of the system, and the cost will be increased.

(3) The leakage reactance of transformer will cause a lot of harmonics in the source voltage of the secondary windings. This makes the phase-locked algorithm more complex.

Based on above analyses, an acquisition winding is set in each phase to obtain the ac voltage of the secondary winding, and the voltage signal is sent to control system of the single-phase PWM rectifier, as shown in Fig. 4. This approach can make up for the above shortcomings and improve the system performance.

D. THE STRUCTURE OF BACK-TO-BACK MODULES

The structure of single-phase back-to-back converter is showed in Fig. 5. It consists of two H-bridge converters whose DC-links are common. L_N is the phase-modulation inductance (it also has the functions of boosting voltage and smoothing), and R_N represents the sum of inductance internal resistance and equivalent resistance of switching loss, while C_1 denotes DC capacitance. C_2, L_2 is the capacitor and the inductance of the double-frequency filter.

The inductance at the input side of the back-to-back converter mainly includes the following functions:

1) Decoupled the source voltage and the input voltage of the rectifier, and realize the energy buffer between the grid and the rectifier.

2) Smooth the source current and obtain the low distorted waveform.

3) Enable the rectifier to have the ability to deal with the active power and the reactive power.

Provided that $u_N = U_{Nm}\sin(\omega t)$, $i_N = I_{Nm}\sin(\omega t - \varphi)$. When the system achieves the unity power factor operation, $\varphi = 0$. According to the energy conservation between the ac side and the dc side

$$u_N i_N = u_{dc} i_d \tag{1}$$

The ac power is

$$\begin{aligned} u_N i_N &= U_{Nm} I_{Nm} \sin(\omega t)\sin(\omega t - \varphi) \\ &= \frac{U_{Nm} I_{Nm}\cos\varphi}{2} - \frac{U_{Nm} I_{Nm}}{2}\cos(2\omega t - \varphi) \end{aligned} \tag{2}$$

It can be seen that the instantaneous power of the dc side consists of two parts. The first one is the dc component, namely the active power of the load, and the second one is the ac component, which is the ripple power on the capacitor. The dc-link power can be expressed as

$$P_{dc} = U_{dc} I_d + C_1 U_{dc} \frac{d\tilde{u}_{dc}}{dt} \tag{3}$$

So

$$C_1 U_{dc} \frac{d\tilde{u}_{dc}}{dt} = -\frac{U_{Nm} I_{Nm}}{2}\cos(2\omega t - \varphi) \tag{4}$$

It can be obtained from (4)

$$\tilde{u}_{dc} = -\frac{U_{Nm} I_{Nm}}{4\omega C_1 U_{dc}}\sin(2\omega t - \varphi) \tag{5}$$

As can be seen from (5), the dc-link voltage contains the double-frequency component. in high-power applications, the double-frequency ripple of the dc link is larger, so double-frequency filter circuit which consists of a inductance L_2 and a capacitance C_2 is employed to eliminate the double-frequency ripple.

The functions of the dc capacitance C_1 include stabilizing the dc voltage, balancing the energy between the ac side and the dc side, and suppressing the harmonic voltage of the dc-link. So, the value of the capacitor should be large enough.

E. ADVANTAGES OF THIS TOPOLOGY

The above analyses indicate this topology can solve the power quality problems of electrified railways, and remove all the neutral sections. Besides, it has the following advantages over other three-phase to single-phase power conversion topologies in traction applications:

(1) The three-phase symmetrical and decoupled structure is more capable of dealing with the negative sequence current problem of electrified railway.

(2) The cascade-parallel structure at the output side allows the employment of switching devices with low voltage and low current stress to obtain the high output voltage and large output current. The cost is reduced and the capacity expansion is easy.

(3) There is no unbalance problem among dc-links owing to the adoption of AFE. Moreover, compared with tri-level converter, the problem of neutral drift does not exist in the dc capacitance.

The superiorities above indicate that it is more applicable to electrified railways.

F. THE DESIGN CALCULATION OF THE MAIN ELEMENTS

This part describes the design and calculation of the main parameters in detail. They are selected according to the unipolar modulation in this paper.

1) THE CAPACITY RATING OF THE TRANSFORMER

Firstly, the capacity rating of the power electronics converter -based traction substation should be determined. As shown in Fig. 1, the magnitude and the phase of the feeder wire can be controlled to dispatch the power flow.

The capacity rating of the traction substation, S_{sk}, is designed by many factors, such as the schedule density on the line and the state of the train. If the line impedance is ignored, the power flow can be divided equally among substations. Assuming that the substation adopts the decentralized power supply, namely, the switches of the section post (SP) which are located between the two substations are open, the power flow of some feeder wire is S_{Lk}, then when the continuous power supply mode is adopted, the minimum capacity of the substation is the average capacity of all the substations. So

$$\min(S_{sk}) = \frac{1}{m}\sum_{k=1}^{m} S_{sk} = \frac{1}{m}\sum_{k=1}^{m} S_{Lk} \tag{6}$$

where, m is the number of the substations.

Because of the dramatic fluctuation of the traction load, the maximum value of S_{Lk} is assumed to be S_{Lkmax}. Regardless of the regenerative energy, $0 \le S_{Lk} \le S_{Lkmax}$. Since each S_{Lk} can not reach the maximum value simultaneously, so

$$\sum_{k=1}^{m} S_{sk} \le \sum_{k=1}^{m} S_{Lk\,\max} \tag{7}$$

The regenerative energy of the train can also be used for the adjacent ones, so the capacity of the traction substation can be designed to be smaller in this condition.

In theory, the capacity rating of the transformer is equal to the capacity rating of the traction substation. There are three multi-wind transformers in this topology, so

$$S_{sT} = \frac{1}{3} S_{sk} \tag{8}$$

where, S_{st} is the capacity of the transformer.

For the general-speed railway, the capacity of the traction substation should be at least 20MVA. For the High-Speed Railway, the capacity of the traction substation should be at least 40MVA. In the next, we take an substation whose capacity is 60MVA as an example to conduct the design calculation of the circuit parameters. The capacity of each transformer is 20MVA. The voltage of the traction network is 27500V.

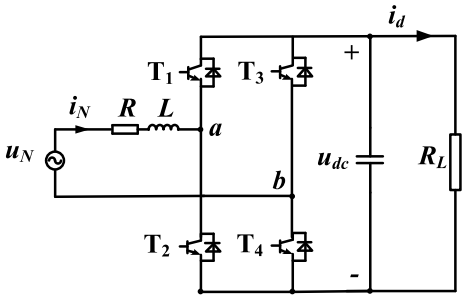

FIGURE 6. The schematic diagram of the single-phase PWM rectifier.

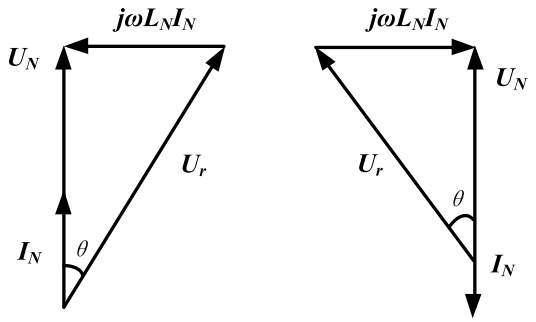

(a) Rectifier condition **(b) Inverter condition**

FIGURE 7. The vector diagram during unity power factor operation.

2) THE SELECTION OF THE SWITCHING DEVICES FOR THE INVERTER

Firstly, we analyze the voltage and current stress of the switching devices.

For the input side, we discuss the switching devices of the PWM rectifier. If the equivalent resistance of the inductance is ignored, the schematic diagram of the single-phase PWM rectifier is shown in Fig. 6.

We can obtain from Fig. 7 that

$$\begin{cases} U_{T1} = U_{T4} = U_{dc}, (T_2 = T_3 = 1)\&\&(T_1 = T_4 = 0) \\ U_{T2} = U_{T3} = U_{dc}, (T_1 = T_4 = 1)\&\&(T_2 = T_3 = 0) \\ U_{T2} = U_{T4} = U_{dc}, (T_1 = T_3 = 1)\&\&(T_2 = T_4 = 0) \\ U_{T1} = U_{T3} = U_{dc}, (T_2 = T_4 = 1)\&\&(T_1 = T_3 = 0) \end{cases} \tag{9}$$

where, "1" represents the switch device is turned on, and "0" denotes that the switch device is turned off.

So, the voltage stress of the switch device is

$$U_{stressn} = U_{dc} \tag{10}$$

When achieving the steady state

$$U_{dc} = U_{dcref} \tag{11}$$

So

$$U_{stressn} = U_{dcref} \tag{12}$$

If we only take the fundamental component of the source current into account, the current stress of the switch device is

$$I_{stressn} = I_{Nm} = \sqrt{2}I_N \tag{13}$$

where, I_N is the root-mean-square (RMS) of the source current.

For the cascade structure of each phase at the output side, the current flowing through each inverter is the same, and it is the output current of each phase.

$$I_o = \frac{S_c}{3U_s} \tag{14}$$

where, S_c is the capacity rating of the system, and U_s is the voltage of traction network.

So, current stress of the switching devices in the inverter is

$$I_{stresso} = \sqrt{2}I_o \tag{15}$$

The voltage stress of the switching devices in the inverter is the same as that of the rectifier.

$$U_{stresso} = U_{dc} = U_{dcref} \tag{16}$$

Take the over-current into account, the current rating of the switching devices is usually selected according to 1.5 to 2 times the RMS of the current flowing through it. the current rating of the switching devices at the output side is

$$I_{switcho} = (1.5 \sim 2)I_o \tag{17}$$

The current rating of the switching device in single-phase PWM rectifier is

$$I_{switchn} = (1.5 \sim 2)I_N \tag{18}$$

Then, we select the voltage rating of the switching device according to its power level. In addition, the switches of the same voltage rating should be adopted in the rectifier and the inverter. In engineering, IGBTs or IGCTs are usually adopted, and the main parameters of the popular versions are shown in TABLE 1.

According to the analysis in this part, we can obtain the following parameters:

1) The output current of each phase is $I_0 = 727$A, and we can select the version of IGBTs in the inverters: 3300V, 1500A.

2) The current stress of the switch devices in the inverters is $I_{stresso} = 1028$A.

TABLE 1. Main parameters of the popular versions for IGBTs and IGCTs.

Switching devices	Parameters
IGBT	600V, 10A~800A
	1200V, 10A~2400A
	1700V, 50A~3600A
	3300V, 200A~1500A
	6500V, 200~750A
IGCT	4500V, 630~5000A
	5500V, 520~3600A
	6500V, 3800A

3) THE REFERENCE VALUE OF DC VOLTAGE

Taking over-voltage into consideration, the voltage rating of the switching device is usually 1.5~2 times of the dc reference value, thus

$$U_{dcref} = \frac{U_{switch}}{1.5 \sim 2} = 1650 \sim 2200\text{V} \tag{19}$$

where, U_{switch} is the voltage rating of the switch device. In addition, we select 1900V as the reference value of the dc voltage. So, the voltage stress of the dc capacitor during steady state is 1900V. moreover, the voltage stress of the switching devices in the inverter and the rectifier is 1900V.

4) THE NUMBER OF MODULES

The maximum output voltage of the cascade inverters each phase can reach NU_{dcref} and it should be greater than the peak amplitude of the traction voltage. Suppose that the modulation ratio $M = 0.98$ and the traction voltage is U_s, then the number of converters is obtained.

$$N > \frac{\sqrt{2}U_s}{MU_{dcref}} = 20.9 \tag{20}$$

In theory, $N = 21$, and In engineering practice, considering the redundancy, the number of modules should be more than the theoretical ones, and usually one or two each phase. So, $N = 22$ or 23. In the simulation and the experiment of this paper, we only conduct the verification of the principle, and does not add the spare modules. So, we select $N = 21$ as the number of modules each phase in the simulation, and the total number is 63.

5) THE SOURCE VOLTAGE OF THE MODULE AND THE SELECTION OF SWITCHING DEVICES FOR RECTIFIER

When the single-phase PWM rectifier achieves the unity power factor operation, the corresponding vector diagram is presented in Fig. 7.

When $u_N = U_{Nm}\sin\omega_N t$, (21) can be obtained.

$$u_r = U_{rm}\sin(\omega_N t - \theta) \tag{21}$$

where, u_r is the fundamental component of the modulation wave. Besides

$$U_{rm} = \frac{U_{Nm}}{\cos\theta} \tag{22}$$

$$I_{Nm} = \frac{U_{Nm}\tan\theta}{\omega_N L_N} \tag{23}$$

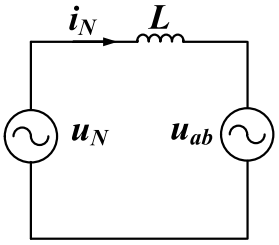

FIGURE 8. The equivalent circuit diagram of the single-phase rectifier.

M is defined as the modulation ratio, so

$$M = \frac{U_{rm}}{U_d} \tag{24}$$

Substituting (24) into (21), (21) can be rewritten as

$$u_r = MU_d \sin(\omega_N t - \theta) \tag{25}$$

Thus

$$MU_d = \frac{U_{Nm}}{\cos\theta} \tag{26}$$

Provided that $u_d = U_{dcref}$ during steady state

$$U_{Nm} = M\cos\theta U_{dcref} \tag{27}$$

We set $U_{Nm} = 950$V according to (27). In addition, the source current of the rectifier is

$$I_N = \frac{S_c}{3U_N} = 1002\text{A} \tag{28}$$

So, we select the version of IGBTs 3300V,1500A for the rectifier.

6) THE PHASE-MODULATION INDUCTANCE

From the analysis in the previous section, we can see that the inductance restricts the active and reactive power of the system absorbed from the grid, and affects the tracking performance of the current. Moreover, it also acts as a filter. we will carry out the calculation of the inductance from the above aspects:

(1) The demand for active power and reactive power

If the equivalent resistance of the inductance is ignored, the equivalent model of the PWM rectifier is shown in Fig.8. Where, $\boldsymbol{u_N}$, $\boldsymbol{i_N}$ and $\boldsymbol{u_{ab}}$ is the source voltage, the source current and the input voltage of the rectifier, respectively.

For simplicity, we only discuss the fundamental components. The vector diagram of the ac side during the steady state is shown in Fig. 9. Where, $\boldsymbol{U_L}$, $\boldsymbol{U_N}$, $\boldsymbol{U_{ab}}$ AND $\boldsymbol{I_N}$ is the voltage vector on both terminals of the inductance, the vector of the source voltage, the vector of the input voltage and the vector of the source current, respectively.

According to the cosines law

$$|U_{ab}|^2 = |U_N|^2 + |U_L|^2 - 2|U_N||U_L|\cos\theta \tag{29}$$

where $\theta = \pi/2$-ϕ, so (29) can be rewritten as

$$|U_{ab}|^2 = |U_N|^2 + |U_L|^2 - 2|U_N||U_L|\cos\phi \tag{30}$$

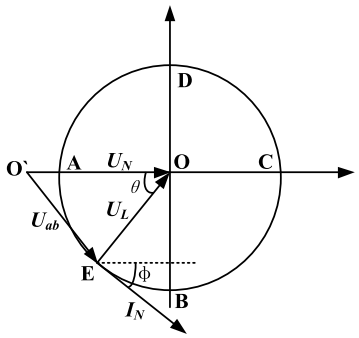

FIGURE 9. The vector diagram of the ac side during the steady state.

The voltage drop on the inductance can be expressed as

$$|U_L| = \omega L_N |I_N| \tag{31}$$

Combining (30) and (31) , (32) can be derived

$$\begin{aligned} L_N &= \frac{|U_N|\sin\phi + \sqrt{|U_{ab}|^2 - |U_N|^2\cos^2\phi}}{\omega I_N} \\ &= \frac{|U_{Nm}|\sin\phi + \sqrt{|U_{abm}|^2 - |U_{Nm}|^2\cos^2\phi}}{\omega I_{Nm}} \end{aligned} \tag{32}$$

where, U_{Nm}, U_{abm}, I_{Nm} is the peak value of the source voltage, the fundamental component of the input voltage and the source current of the PWM rectifier. MU_{dc} is the peak value of the input voltage. So

$$U_{abm} \le MU_{dc} \tag{33}$$

Substituting (33) into (32), (34) can be obtained

$$L_N \le \frac{|U_{Nm}|\sin\phi + \sqrt{M^2U_{dc}^2 - |U_{Nm}|^2\cos^2\phi}}{\omega I_{Nm}} \tag{34}$$

When achieving the unity power factor operation, $\phi = 0$, in this condition the value of the inductance is

$$L_N \le \frac{\sqrt{M^2U_{dc}^2 - |U_{Nm}|^2}}{\omega I_{Nm}} = 4.1mH \tag{35}$$

(2) The demand for the transient current tracking

The inductance of the rectifier needs to meet the current tracking requirement, which means that the current must be tracked rapidly and the harmonic component of the current must be suppressed.

For the transient process of current tracking, the highest gradient occurs at the zero point, where the inductance should be small enough to track the source current. The waveform of one switching cycle at zero crossing point is shown Fig.10.

When $0 \le t \le T_1$

$$U_N - U_{ab} = U_{dc} = L_N\frac{d_{i_1}}{d_t} \approx L_N\frac{\Delta i_1}{T_1} \tag{36}$$

So

$$\Delta i_1 = U_{dc}\frac{T_1}{L_N} \tag{37}$$

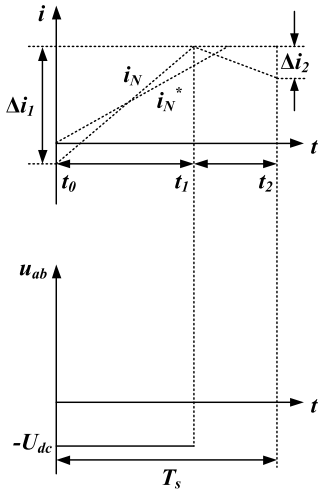

FIGURE 10. The waveform of one switching cycle at zero-crossing point.

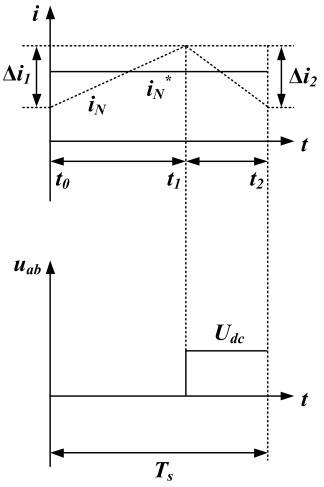

FIGURE 11. The waveform of one switching cycle at the peak value.

When $T_1 \le t \le T_2$

$$L_N \frac{\Delta i_2}{T_1} = 0 \tag{38}$$

In order to meet the requirement of transient current tracking

$$\frac{\Delta i_1 - \Delta i_2}{T_s} \ge \frac{I_{Nm} \sin \omega T_s}{T_s} \tag{39}$$

When $f_s \ge 2$kHz

$$\sin \omega T_s \approx \omega T_s \tag{40}$$

So

$$L_N \le \frac{U_{dc} T_1}{I_{Nm} \omega T_s} \tag{41}$$

When the tracking speed of the source current achieves the fastest, the duty cycle reaches the maximum. When $T_1 = T_S$ the value of the inductance should meet (42)

$$L_N \le \frac{U_{dc}}{I_{Nm} \omega} = 4.27mH \tag{42}$$

At the peak of the source current, the harmonic content is the highest, and the value of the inductance should be as large as possible to suppress the harmonic of the source current. The waveform of one switching cycle at the peak value of the current is shown Fig.11.

When $t_0 \le t \le t_1$

$$U_N - U_{ab} = U_N \approx L_N \frac{\Delta i_1}{T_1} \tag{43}$$

So

$$\Delta i_1 \approx \frac{T_1 U_N}{L_N} \tag{44}$$

When $t_1 \le t \le t_2$

$$U_N - U_{ab} = U_N - U_{dc} \approx L_N \frac{\Delta i_2}{T_2} \tag{45}$$

In order to meet the requirement of transient current tracking,

$$\Delta i_2 \approx \frac{T_2 (U_N - U_{dc})}{L_N} \tag{46}$$

Provided that the maximum fluctuation value is $\Delta i_{N\,\max}$, thus

$$|\Delta i_1| = |\Delta i_2| \le \Delta i_{\max} \tag{47}$$

Substituting (44) and (46) into (47)

$$L_N \ge \frac{(U_{dc} - U_{Nm})\, U_{Nm} T_s}{U_{dc} \Delta i_{\max}} = 0.98mH \tag{48}$$

Assume that fs=2kHz. Combine (35), (42) and (48), the range of the inductance value is

$$0.98mH \le L_N \le 4.1mH \tag{49}$$

We select $L_N = 1.2mH$. In the simulation, we select the lower switching frequency fs=500Hz to reduce the loss caused by the switching devices. in this condition, total harmonic distortion (THD) of the source current will be higher in a single module. But thd of the grid current reaches the standard because of the high equivalent switching frequency obtained from PS-SPWM.

7) THE DC-LINK DOUBLE-FREQUECY FILTER

Because the train is a single-phase ac load, dc voltage contains double-frequency (100Hz) component. 100 Hz ripple component should be eliminated because if not, the triple-frequency component will be introduced to the source current. Double-frequency filter which consists of a inductance and a capacitance in series is adopted in the dc-link to remove it. So

$$2\omega = \frac{1}{\sqrt{L_2 C_2}} \tag{50}$$

The current of the filter circuit is

$$i_{d2} = \frac{U_N I_N}{U_d} \sin(2\omega t) = I_{d2m} \sin(2\omega t) \tag{51}$$

where, I_{d2m} is the peak value of the double-frequency current. the peak value of the voltage on the capacitor C_2 is

$$U_{C2m} = U_d + \frac{I_{d2m}}{2\omega C_2} \tag{52}$$

Generally, $U_{c2m} = 1.1U_d$ in engineering. So

$$C_2 \geq \frac{I_{d2m}}{2\omega\left(U_{C2m} - U_d\right)} = 4200\mu F \tag{53}$$

We select $C_2 = 6000\mu F$, then $L_2 = 0.423mH$.

8) THE DC-LINK CAPACITANCE

The dc capacitance C_1 is an important device to balance the energy between the grid and the dc side. Since the double-frequency filter has been employed on the dc-link, the capacitance C_1 is related to the change of energy storage in the inductance on grid side. The fluctuation of the voltage on the capacitor is caused by the energy deviation between the input side and the output side. According to the law of energy conservation, the maximum energy ripple on the capacitor is equal to the maximum energy ripple of the switching frequency current on the grid side. So

$$\begin{aligned}&\frac{1}{2}L_N(I_{Nm} + \frac{1}{2}\Delta i_{Nm})^2 - \frac{1}{2}L_N(I_{Nm} - \frac{1}{2}\Delta i_{Nm})^2 \\ &\quad = \frac{1}{2}C_1(U_d + \frac{1}{2}\Delta U_{dm})^2 - \frac{1}{2}C_1(U_d - \frac{1}{2}\Delta U_{dm})^2\end{aligned} \tag{54}$$

The value of the capacitor C_1 can be calculated from (54) and it can be expressed as

$$C_1 \geq \frac{L_N r_1 I_{Nm}^2}{r_2 U_d^2} \tag{55}$$

where, r_1 is the coefficient of the source current ripple, and r_2 is the coefficient of the dc voltage ripple. Suppose that $r_1 = 0.2$ and $r_2 = 0.05$, then $C_1 \geq 5346\ \mu F$, and we select $C_1 = 6000\ \mu F$.

9) THE INDUCTANCE AT THE OUTPUT SIDE

It can be seen from the previous analysis that we should consider the active and reactive power requirements of the load and the harmonic content of the output voltage for the selection of inductance. According to the inductance selection method of the PWM rectifier, the inductance needs to meet (56) for the load active and reactive power demand

$$L_S \leq \frac{|U_{sm}|\sin\phi + \sqrt{M^2U_{dcm}^2 - |U_{sm}|^2\cos^2\phi}}{\omega I_{sm}} \tag{56}$$

where, U_{sm} is the peak value of the voltage of traction network, I_{sm} is the peak value of the output current, and U_{dcm} is the sum of the dc voltages of cascade inverters in each phase.

When the harmonic content achieves the requirement, the value of the inductance should meet

$$L_S \geq \frac{(U_{dcm} - U_{sm})\,U_{sm}T_s}{U_{dcm}\Delta i_{s\max}} \tag{57}$$

where, U_s is the voltage of traction network, Δi_{smax} is the maximum fluctuation of the output current in each phase.

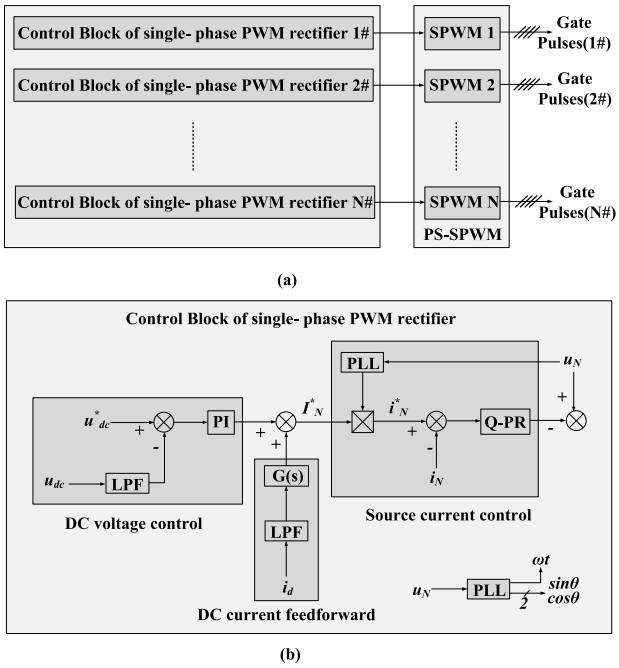

FIGURE 12. The control diagram of the input side. (a): Overall control diagram of the input. (b): The control block of the single-phase PWM rectifier.

We need to know the power factor of the load. assume that the load is pure resistive, then $\phi = 0$, in this condition the value of the inductance meet

$$3.52mH \leq L_S \leq 18mH \tag{58}$$

We set it to $6.4mH$.

III. CONTROL OF THE PROPOSED TOPOLOGY

The main work of this section, briefly, is to design the control system of the proposed structure. According to the analysis in Section **II**, dc voltage should be stable to ensure the power balance between the power grid and the load. The control of the input side and that of the output side is independent because of decoupling characteristics. We can introduce the control of the input side and that of the output side, respectively.

A. CONTROL BLOCK OF THE INPUT SIDE

For the input side of the system, the single-phase PWM rectifier can regulate dc voltage and the source current, and PS-SPWM should be adopted to reduce THD of the source current at the PCC. Thereby, the control targets at the input side of the system include dc voltage control, unity power factor, and the harmonic elimination at the PCC. The mathematical model of the single-phase PWM rectifier is presented in (59) from Fig. 6.

$$\begin{cases} u_N = Ri_N + L\dfrac{di_N}{dt} + Su_{dc} \\ Si_N = C\dfrac{du_{dc}}{dt} + \dfrac{u_{dc}}{R} \end{cases} \tag{59}$$

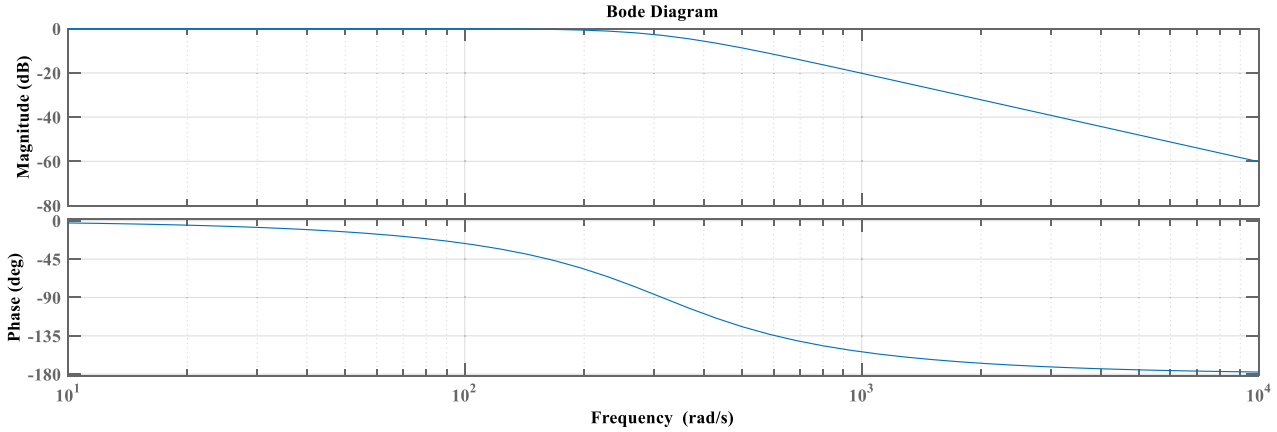

FIGURE 13. The bode diagram for the transfer function of the second-order butterworth low pass filter.

where

$$S = \begin{cases} -1, & (T_2 = T_3 = 1)\&\&(T_1 = T_4 = 0) \\ 1, & (T_1 = T_4 = 1)\&\&(T_2 = T_3 = 0) \\ 0, & (T_1 = T_3 = 1)||(T_2 = T_4 = 1) \end{cases} \tag{60}$$

The control of the input side is shown in Fig. 13(a). The control block of the single-phase PWM rectifier is shown in Fig. 13(b), and it mainly consists of dc voltage control and the source current control. In addition, the dc current feedforward link is added in the control block to improve the dynamic performance of the system for the impact load. This subsection focuses on four parts as follows.

1) DC VOLTAGE CONTROL

The rectifier controls dc voltage to follow the voltage reference to keep it stable. In order to obtain the dc signal without the double-frequency ripple, low pass filter (LPF) is employed, and its cut-off frequency should be under 100Hz. But, too low cut-off frequency is not allowed because it will degrade the dynamic performance of the system. Proportional integration (PI) controller, expressed as $K_P + K_I/s$, is introduced to regulate dc voltage since it can control the dc component with no steady state error in theory.

For the LPF, the second-order filter show the better performance than the first-order filter. So, we adopt the second-order Butterworth low pass filter, and its transfer function is

$$G_F(s) = \frac{\omega_0^2}{s^2 + 2\varsigma\omega_0 s + \omega_0^2} \tag{61}$$

where, the damping ratio $\varsigma = 0.707$, and ω_0 is the cut-off frequency. In general, the cut-off frequency should not be under 50Hz. The bode diagram of (61) is shown in Fig.14.

It can be seen that in the low frequency band which is under the cut-off frequency, the amplitude gain is 1 and the dc signal will be obtained without attenuation. Over the cut-off frequency, the amplitude curve attenuates rapidly with the slope of -40 dB/dec, and the harmonics above double-frequency can be filtered.

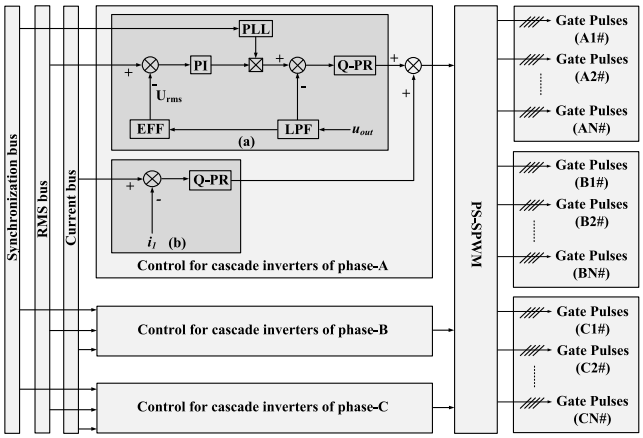

FIGURE 14. The control diagram of the output side. (a): Control for the output voltage. (b): The current sharing control.

2) DC CURRENT FEEDFORWARD CONTROL

In the ac-dc-ac structure, the inverter is equivalent to a dc load of the rectifier, as shown in Fig. 7. The train is an impact load, and it will cause the mutation of dc current, thus worsen the dynamic response of dc voltage. DC current feedforward is adopted in the control block of the rectifier to improve the dynamic performance to dc current mutation. LPF is also used to filter the 100Hz ripple component of dc current. G(s) is the transfer function of dc current feedforward link, and

$$G(s) = K_i(T_i s + 1) \tag{62}$$

where, K_i is the proportion coefficient, and T_i is the differential time which includes filtering delay, the delay caused by current loop, and the modulation delay, and so on.

According to the power balance between the rectifier and the inverter

$$\frac{U_N I_N}{2} = U_{dc} I_d \tag{63}$$

where, I_d is the dc component without double-frequency ripple. So,

$$K_i = \frac{I_N}{I_d} = \frac{2U_{dc}}{U_N} \tag{64}$$

3) SOURCE CURRENT CONTROL

The sum of dc voltage loop output and dc current feed-forward output is taken as the amplitude reference of the source current. Phase-Locked-Loop (PLL) is used to synchronize with the source voltage. Where, the source voltage singal is acquired from the acquisition winding. It only deal with signal acquisition, so the voltage signal obtained is little distorted. This provides convenience for the phase angle synchronization. Quasi-proportional resonance (Q-PR) controller is used to control the source current because it can regulate the ac component with on steady state error in theory and it is easy for application. It can be written as

$$G_{PR}(s) = K_P + \frac{2K_r\omega_c s}{s^2 + 2\omega_c s + \omega_0^2} \tag{65}$$

where, K_P is the proportion coefficient. ω_0 and K_r are the desired resonant frequency and the resonant gain, respectively. ω_c is the cut-off frequency.

B. CONTROL BLOCK OF THE OUTPUT SIDE

For the output side of the system, the cascade inverters should control the output voltage to supply the traction load, and the current sharing among three phases should be realized. The control diagram of the output side is shown in Fig. 14. Synchronization bus and root-mean-square (RMS) bus provide the phase reference and RMS reference for output voltage of each phase, respectively. This can reduce the difference among the output voltages of three phases to a certain extent. Current bus offers the average instantaneous current as the current reference. This part consists of two main blocks as follows.

1) CONTROL FOR THE OUTPUT VOLTAGE

Aiming at the traction load with the nonlinear and impact characteristics, a nice sine degree and stable voltage is necessary. So, the output voltage should be controlled. Where, the control for RMS and the control for the instantaneous value is included, presented in Fig. 15(a).

Controlling RMS of the output voltage can reduce the steady state error to obtain a stable output voltage. LPF is used to smooth the output voltage of the cascade inverters. EFF block is employed to calculate RMS of the output voltage. PI controller is introduced to make it track the reference value acquired from RMS bus. The control loop for the instantaneous value of output voltage can improve the waveform quality and dynamic response in case of the non-linear and impact loads. Q-PR controller is used to reduce the steady state error for ac component.

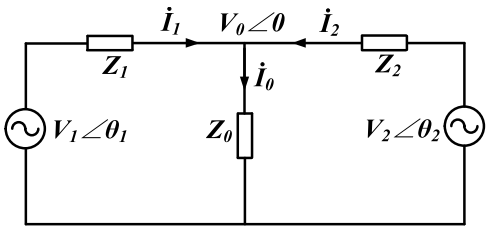

FIGURE 15. The schematic diagram of two inverters in parallel.

2) CURRENT SHARING CONTROL

As can be seen from Fig. 2, it adopts parallel structure to expand the capacity of the system at the output side. Circulating current suppression plays an important role in the parallel structure of inverters. The single-phase cascade inverter in this structure is equivalent to a single-phase voltage source, and the circulating current characteristics is analyzed by parallel operation of two inverters, as shown in Fig. 15.

We can obtain (66) from Fig. 15

$$\begin{cases} \dot{V}_1 - Z_1\dot{I}_1 = V_0 \\ \dot{V}_2 - Z_2\dot{I}_2 = V_0 \end{cases} \tag{66}$$

Assuming that $Z_1 = Z_2 = Z$, (67) can be derived

$$\begin{cases} \dot{I}_1 - \dot{I}_2 = \dfrac{\dot{V}_1 - \dot{V}_2}{Z} \\ \dot{I}_1 + \dot{I}_2 = \dfrac{\dot{V}_1 + \dot{V}_2 - 2V_0}{Z} \end{cases} \tag{67}$$

Thus

$$\begin{cases} \dot{I}_1 = \dfrac{V_0}{2Z_0} + \dfrac{\dot{V}_1 - \dot{V}_2}{2Z} \\ \dot{I}_2 = \dfrac{V_0}{2Z_0} - \dfrac{\dot{V}_1 - \dot{V}_2}{2Z} \end{cases} \tag{68}$$

As presented in (68), the output current of each inverter consists of two parts. One is the load current this inverter provides, the former part of (68) and the other is the circulating current, the latter part of that. So, the expression of the circulating current is

$$\dot{I}_h = \frac{\dot{V}_1 - \dot{V}_2}{2Z} = \frac{\dot{I}_1 - \dot{I}_2}{2} \tag{69}$$

It can be seen that the load current must be shared so that the circulating current can be suppressed. In this way, the amplitude, phase and frequency of the output voltages can be consistent.

Even if the uniform RMS and the phase references of the output voltage are provided for the output voltage regulation, the magnitude and phase of the output voltages among inverters will be different for the reasons such as control accuracy, component parameters, trigger angle and conduction time of the switching devices. This will result in circulating current. Circulating current will lower the loading capacity, and degrade the efficiency and reliability of the system. Excessive circulating current will threaten the normal operation of the system and even damage the switching devices.

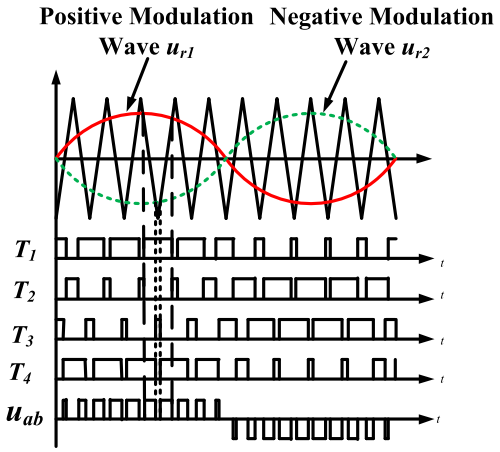

FIGURE 16. The schematic diagram of the unipolar double-frequency spwm.

In Fig. 15(b), the current reference provided by current bus is expressed as

$$i_{ref} = \frac{1}{N}\sum_{m=1}^{N} i_m \tag{70}$$

where, N is the number of parallel inverters that are put into operation.

Current deviation is calculated by Q-PR controller, and it is compensated to the reference voltage of each phase to eliminate the unbalance among the output currents. Thus, the load current will be shared equally among the inverters, and the magnitude and phase of the output voltages among inverters will be the same. This control method is simple and easy to implement.

The control strategy designed in this section provides convenience for this topology used in electrified railways.

C. MODULATION STRATEGY FOR THE CASCADE STRUCTURE

For the cascade structure, unipolar double-frequency carrier-phase-shift SPWM (CPS-SPWM) technology is adopted. It is the combination of unipolar double-frequency modulation and the CPS-SPWM technology. The schematic diagram of the unipolar double-frequency SPWM is shown in Fig. 16. The phase difference between the positive and negative modulation wave is π. They are compared with the same carrier wave simultaneously, then the driving signals of switching devices T1, T2, T3 and T4 are obtained. The principle of CPS-SPWM technology is that in multi-module structure, the carrier phase of adjacent converter differs by $T/2N$ in turn, where T is the carrier cycle and N is the number of modules.

The dual Fourier expression for the output voltage of the cascade converter is

$$\begin{aligned} F(t) = {} & NMU_{dc}\sin(\omega_s t+\varphi) \\ & + \frac{4U_{dc}}{\pi}\sum_{m=2,4,\ldots}^{\infty}\sum_{n=\pm1,\pm3,\ldots}^{\pm\infty}\frac{J_n(\frac{m}{2}M\pi)}{m} \\ & (-1)^{\frac{m}{2}}\sin[m(\omega_c t+\frac{\pi}{N})+n(\omega_s t+\varphi)] \end{aligned} \tag{71}$$

TABLE 2. Main simulation parameters of the traditional traction power supply systems.

Main Parameters	Value
Nominal primary voltage of SCOTT transformer	110kV
Nominal secondary voltage of SCOTT transformer	27.5kV
Load in α phase	20 Ω
Load in β phase	40 Ω

where, M, ω_c and ω_s is the modulation ratio, the angular frequency of the carrier wave and the angular frequency of the fundamental wave, respectively.

The conclusions can be derived from (71) as follows:

(1) The amplitude of the fundamental component of the output voltage is N times that of a single converter, and the phase of it is not changed.

(2) The lowest harmonic locates in $2Nf_c+nf_s$, so the equivalent switching frequency is increased to $2N$ times.

Therefore, the level of the output voltage is increased and the harmonic content of that is reduced greatly.

IV. SIMULATION AND EXPERIMENTAL RESULTS

A. SIMULATION RESULTS AND ANALYSIS

Simulation was carried out by MATLAB/SIMULINK in this section to verify the proposed topology. It is worth noting that for display purposes, the magnitudes of the primary voltages in the multi-winding transformers are zoomed out to 1/300 of the original ones, while the output voltage and the load voltage are zoomed out to 1/100 of the original ones. The load current is zoomed out to 1/10 of the original one. In the harmonic analysis, the fundamental component was withdrawn and we set the vertical axis between 0 and 0.5 to facilitate the presentation of harmonic content.

Firstly, the simulation for the traditional power supply systems was conducted. In the traditional traction power supply systems, the SCOTT transformer was adopted, and the main parameters are presented in TABLE 2. In the simulation results, the power quality problems are indicated.

Then, the simulation for the proposed scheme is conducted and the main parameters are shown in TABLE 3. In order to evaluate the dynamic performances, two resistances where each one is 40 Ω are paralleled as the load and they are put into operation at the time of 0.2s and 0.6s, respectively. It is compared with the traditional scheme to verify its ability to solve the power quality problems of electrified railways. The controller parameters in the proposed system for the simulation is presented in TABLE 4.

1) SIMULATION RESULTS FOR THE POWER QUALITY AT THE PCC

In traditional traction power supply systems, negative sequence current is the main power quality problem and we regard it as the comparison object. The grid currents of the traditional traction power supply are shown in Fig. 17(a).

TABLE 3. Main simulation parameters of the proposed scheme.

Main Parameters	Value
Primary/ Secondary voltage of transformer	110kV/950V
DC capacitor C_1	6000 μ F
LC double-frequency filter L_2	0.423mH
LC double-frequency filter C_2	6000 μ F
DC voltage reference	1900V
Phase-modulation inductance of each module	1.2 mH
Switching frequency (input side/output side)	500 Hz
Number of modules	63
Smoothing inductor of each phase(output side)	6.4 mH
Capacity	63MVA
The output voltage	27.5 kV

TABLE 4. Controller parameters of the proposed scheme for the simulation.

Controller Parameters	Value
DC voltage controller	K_p=0.5, K_I=2
Source current controller	K_p=0.5, K_r=56, ω_c =5, ω_0 =100*pi
Voltage controller for the RMS of the output voltage	K_p=0.8, K_I=50
Voltage controller for the instantaneous value of the output voltage	K_p=2, K_r=100, ω_c =5, ω_0 =100*pi
Current sharing controller	K_p=3, K_r=60, ω_c =5, ω_0 =100*pi

The maximum amplitudes of the source currents reach 290A, and the minimum amplitudes of these are 160A, so the unbalance degree of the grid currents is very high. Fig. 17(b) presents the grid currents in the proposed scheme, and the unbalance degree is very low, so the negative sequence current is suppressed. The source voltage and the source current of phase-A are shown in Fig. 17(c). The phase of source current can synchronize that of the source voltage very well to achieve unity power factor operation. That is to say, the system absorbs no reactive power from the grid. The harmonic analysis for the source voltage is shown in Fig. 18(a), and it indicates that no harmonic current is injected into the power grid.

The above analysis indicates that the problem of the negative sequence current is solved and the power quality at PCC is not degraded during operation.

2) SIMULATION RESULTS FOR THE OUTPUT SIDE OF THE SYSTEM

Fig. 17(d) presents the output voltages. It can be seen that the voltage wave is a multi-level staircase and the sine degree is very nice. The more the converters in the cascade structure, the lower requirements will be for filter circuit design. When the cascade number is high enough, it is possible to omit the filter circuit to connect the traction network directly.

The load voltage and its RMS curve are shown in Fig. 17(e) and Fig. 17(f) respectively, and the harmonic analysis for the load voltage is shown in Fig. 17(h). We can see that the load obtains a stable voltage whose RMS is 27.5kV with low THD to ensure normal operation. When the load current is increased, the load voltage will decline slightly, but it can return to the reference value quickly.

Meanwhile, Fig.17 shows that the system has nice dynamic performance.

3) SIMULATION RESULT FOR DC VOLTAGE

DC voltage of the module NO.1 in phase-A is studied as the object, and the simulation result is shown in Fig. 18. As can be seen, little overshoot is presented and it can be stable around reference value 1900V, so the power absorbed from the public grid can be transmitted to the load totally on the condition that the loss is ignored. When the load current increases, the dc voltage will decrease, but it can return to the reference value quickly, which proves the effectiveness of dc voltage control.

4) SIMULATION RESULTS FOR THE VALIDITY OF CURRENT SHARING CONTROL

In Fig. 19(a), it indicates that in steady state, the circulating current is small and it does not impact on the normal operation of the system. But in the transient state, such as startup process, the load mutation, the excessive circulating current will deteriorate the system performance and even damages the power devices. So, the current sharing control is necessary.

The current sharing control is adopted in Fig. 19(b). It shows that the circulating current is suppressed significantly that the system can work well. Fig. 19(c) presents the circulating current between phase-A and phase-B with the current sharing control. It can be seen that when the system starts with no load, circulating current occurs because of the transient state, but it was not big, and the amplitude did not exceed 5A. The system is stable at about 0.1s, and the amplitude of the circulating current was about 3A. After 0.2s, the load was put into, so the output currents were increased, and at about 0.4s it reaches the steady state, the circulating increased to about 5A. At the time of 0.6s, another resistance was put into, and the output current increased. At about 0.8s the system reaches the steady state, the circulating current increases to about 10A. In the whole process, the maximum circulating current is about 10A, and the amplitude of the output current of each phase is about 650A. So the ratio is about 1.5%, which meets the requirements.

B. EXPERIMENTAL RESULTS AND ANALYSIS

In order to further verify the performances of the system, a prototype whose specifications are presented in TABLE 5 was evaluated.

The diagram of the prototype and the hardware structure of control system are displayed in Fig. 20. The power circuit of the prototype which is fed by the auxiliary power

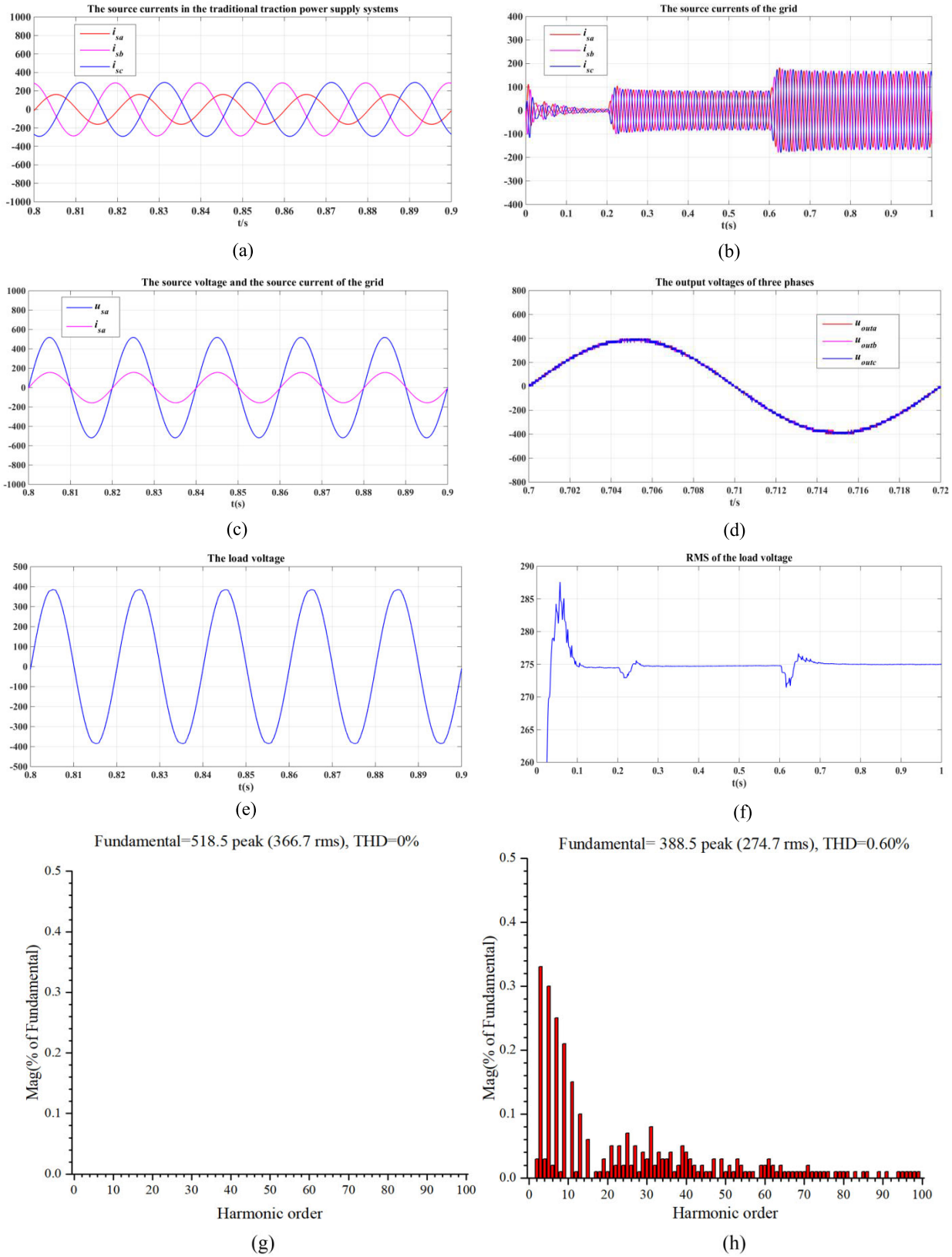

FIGURE 17. The simulation results for basic functions and the harmonic analysis. (a): The grid currents in the traditional traction power supply systems. (b): The grid currents in the proposed scheme. (c): The grid voltage and the grid current of phase-A. (d): The output voltages. (e): The load voltage. (f): RMS curve of the load voltage. (g), (h): The harmonic analysis for the grid voltage and the load voltage, respectively.

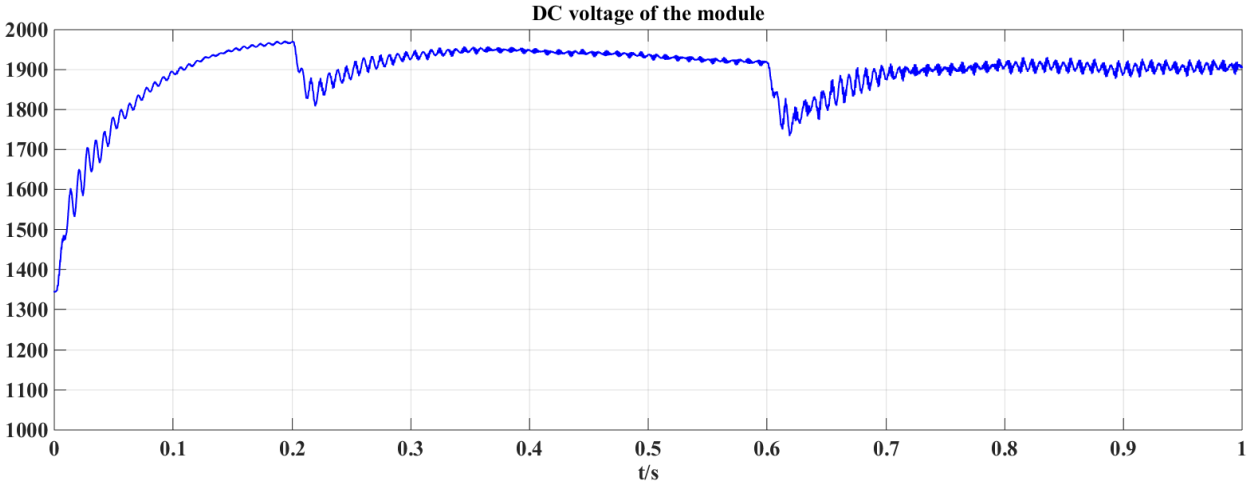

FIGURE 18. The simulation results for DC voltage.

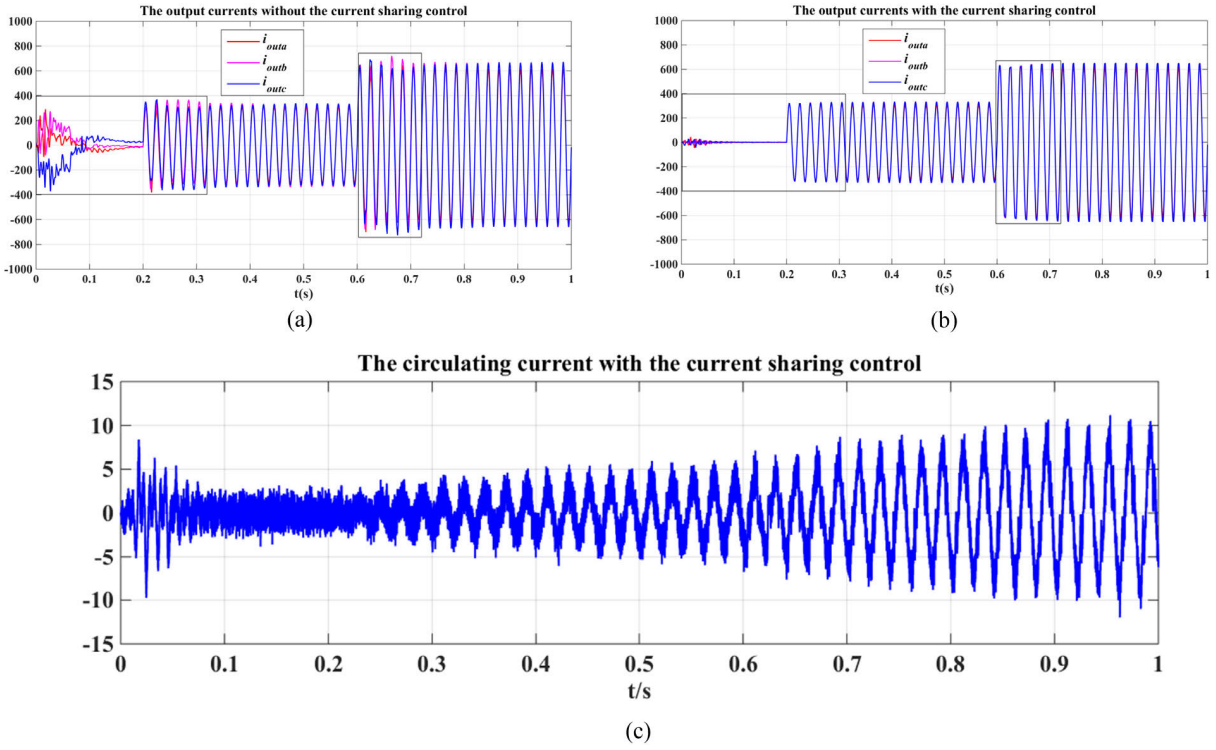

FIGURE 19. The simulation results for the current sharing control. (a): The output currents without current sharing control. (b): The output currents with current sharing control. (c): The circulating current between phase-A and phase-B with the current sharing control.

mainly includes three multi-winding transformers, eighteen power modules where one is redundant each phase, three smoothing inductances. The hardware sructure of the control system includes three parts. One is the power module control board which is mainly responsible for signal acquisition, control and protection of the single-phase PWM rectifier at the input. It is composed of three chips (i.e. an AD chip that manages the signal acquisition, a CPLD chip which sends PWM pulses and protects the power cell, and a DSP chip whose model is TMS320F2812 that performs the control algorithm of the power cell). Another is the master control board which consists of two FPGA chips (i.e. the master chip mainly conducts the signal acquisition and system protection, while the slave chip handles the modulation and communication with the power cell) and two DSP chips (i.e. the master chip whose model is TMS320C6748 is responsible for the control algorithm, and the slave chip whose model is TMS320F28335 performs the communication with host PC.

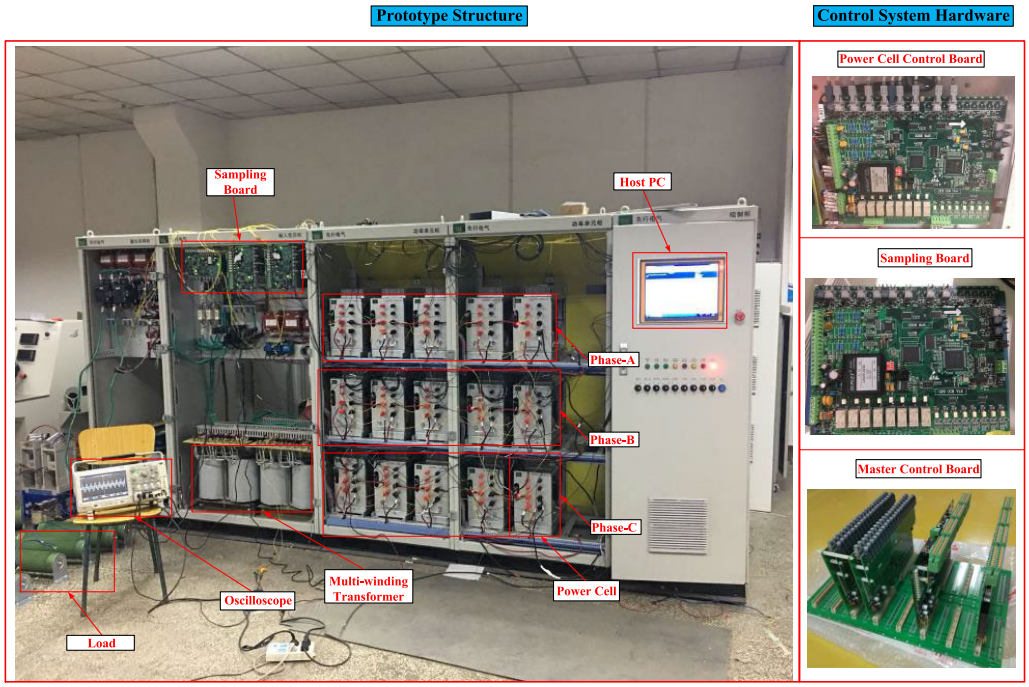

FIGURE 20. The experimental setup.

TABLE 5. Main experimental parameters.

Parameters	Value
Nominal primary voltage of multi-winding transformer	220V
Nominal secondary voltage of multi-winding transformer	95V
DC capacitor	4700μF
DC voltage reference	190V
Phase-modulation inductance of each module	0.6mH
Switching frequency (input side/output side)	2k Hz
Number of modules	15
Smoothing inductor of each phase(output side)	12mH
Nominal capacity	45kVA
Nominal output voltage	675V

The last one is the sampling board which deals with the signal acquisition of the voltage in the secondary side of the multi-winding transformer and sends carrier phase shift signals. Six paralleled resistances where each one is 60 Ω and a 2mH inductance which is in series with the paralleled resistances are selected as the load. The controller parameters in the proposed system for the experiment are presented in TABLE 6.

Meanwhile, the experiment for the traditional traction power supply systems was also carried out. We adopted SCOTT transformer, and the parameters are shown in TABLE 7.

In order to display harmonic content intuitively, the same method was used as in simulation, and the vertical axis was set between 0 and 2.

TABLE 6. Controller parameters of the proposed scheme for the experiment.

Controller Parameters	Value
DC voltage controller	K_p=1.46, K_I=190
Source current controller	K_p=4.9, K_I=2000
Voltage controller for the RMS of the output voltage	K_p=1.8, K_I=146
Voltage controller for the instantaneous value of the output voltage	K_p=4.6, K_I=1140
Current sharing controller	K_p=5.2, K_I=1280

TABLE 7. Main experimental parameters of the traditional traction power supply systems.

Main Parameters	Value
Nominal primary voltage of SCOTT transformer	220V
Nominal secondary voltage of SCOTT transformer	275V
Load in α phase	20Ω
Load in β phase	40Ω

It is worth noting that in order to limit the current flowing through the resistance, we use a voltage regulator to adjust the primary voltage of the transformer to 110V. As shown in Fig. 21(a), the three-phase currents show an asymmetric state. The current of phase-A is smaller, with amplitude around 3A. The currents of phase-B and phase-C are larger, reaching 7A and 7.4A, respectively. So, the unbalance degree of three phases is high. Since the load is linear, it injects little reactive current or harmonic current into the grid, which can

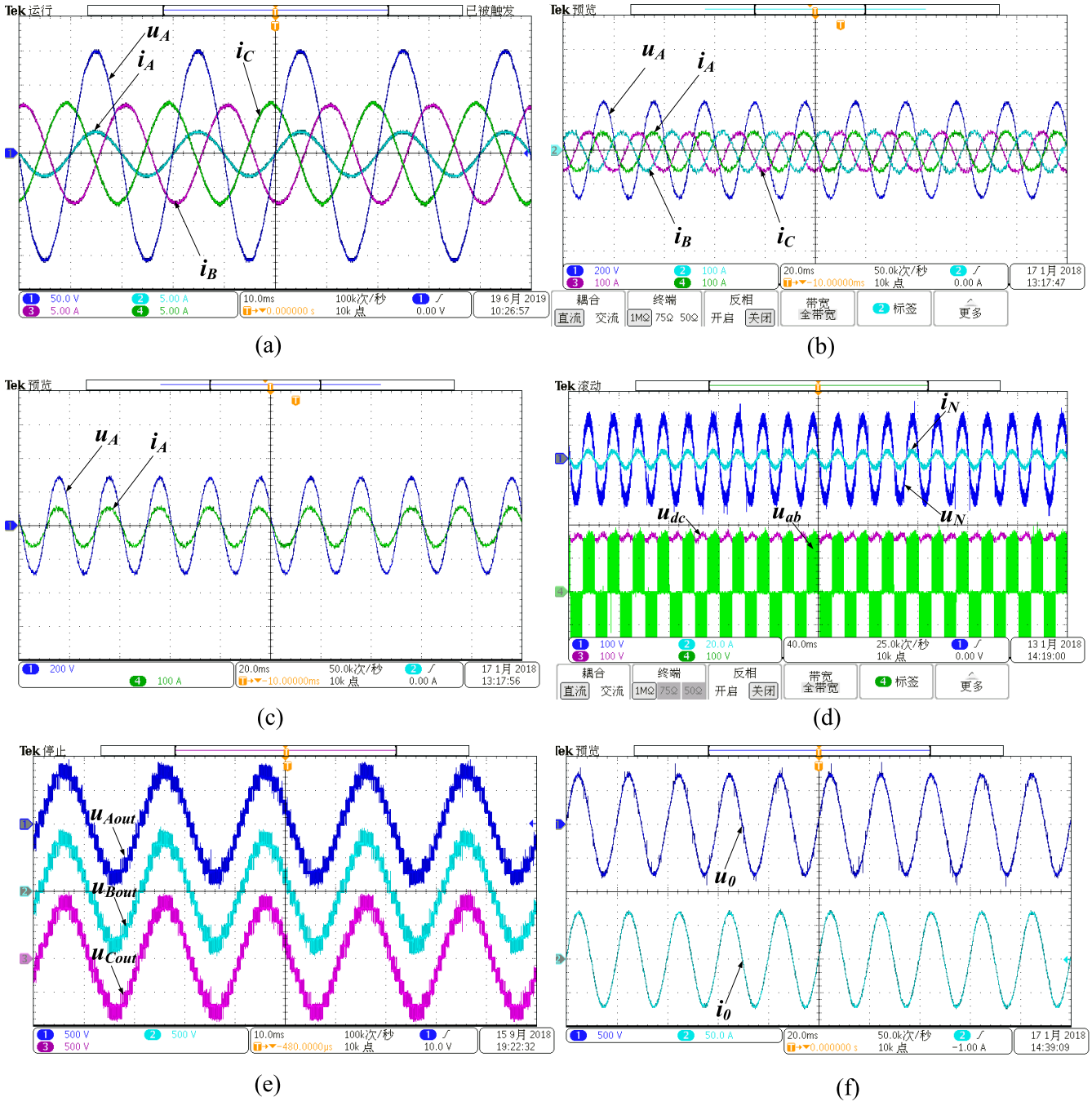

FIGURE 21. The experimental results during the steady state. (a): The grid voltage and the grid currents in the traditional traction power sypply systems. (b): The grid voltage and the grid currents in the proposed system. (c): The grid voltage and the grid current of phase-A. (d): The waveforms of the single-phase PWM rectifier. (e): The output voltages. (f): The load voltage and the load current.

also be seen from the phase angle difference between the grid voltage and the grid current of phase-A, and the sinusoidal degree of grid voltage. Therefore, the problem of the negative sequence current is more prominent. The Fig. 21(b) shows the waveforms of the grid-voltage of phase-A and the grid currents. It can be seen that the grid currents are symmetrical and the unbalance degree is very low. In order to highlight the phase relationship between the grid voltage and the grid current more clearly, Fig. 21(c) shows the grid voltage and the grid current of phase-A. It can be seen that the phase of the current synchronizes that of the grid voltage, and the phase angle difference is very small, so the high power factor operation is achieved. It indicates that the system absorbs little reactive current from the grid during operation. Harmonic analysis for the grid voltage is carried out in Fig. 22(a). THD of the grid voltage is under 5%, so it meets the standard.

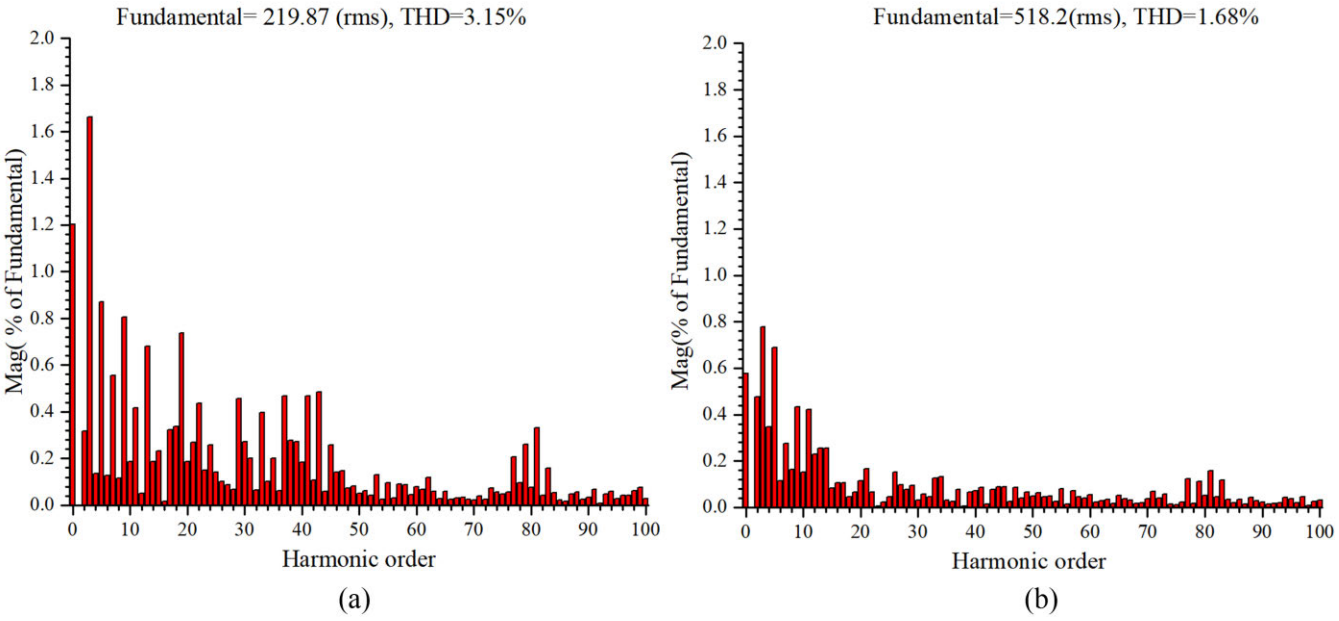

FIGURE 22. The harmonic analysis. (a), (b): The harmonic analysis for the grid current of phase-A and the load voltage, respectively.

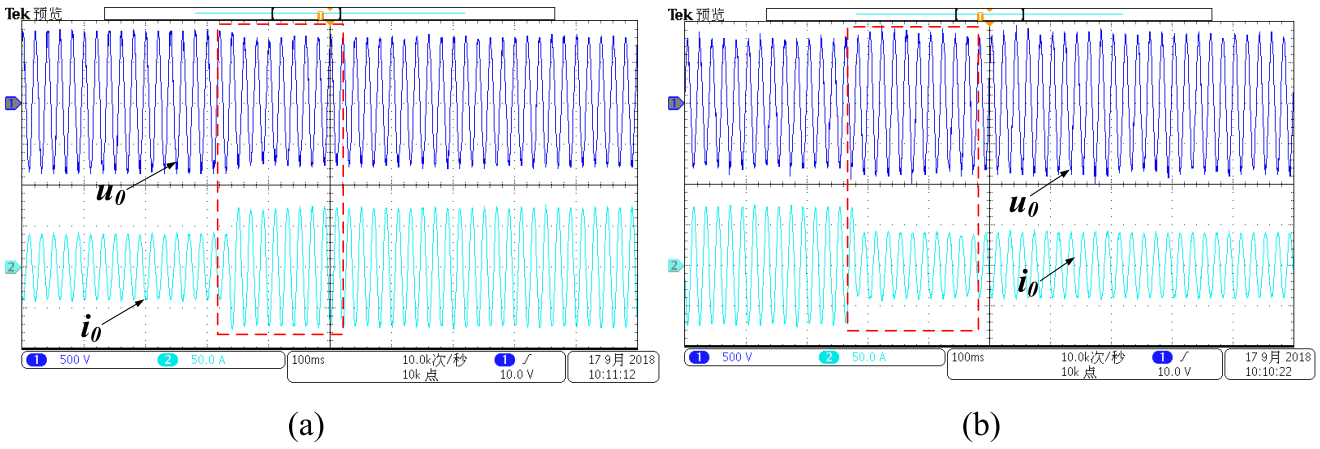

FIGURE 23. The dynamic responses of the system. (a): The load voltage and the load current when the operation state switches from light load to heavy load. (b): The load voltage and the load current when the operation state switches from heavy load to light load.

The above analysis shows that the system improves the power quality problem at the PCC. Fig. 21(d) shows the waveforms of the single-phase PWM rectifier. Generally speaking, dc voltage is stable, but the double-frequency component is larger. The first reason is that there is no double-frequency filter installed on the low-power platform, and the second reason is that the capacitance is small and the voltage stability performance is weak. Fig. 21(e) shows the waveforms of the output voltages. It can be seen that the output voltages present a multi-level staircase, whose level is 11 (2N+1, N=5). Moreover, compared with the waveforms of output voltages in the simulation, it can be seen that increasing the number of modules can improve the sinusoidal degree of output voltages and reduce the load of the filter. This verifies the conclusion in the simulation. Fig. 21(f) presents the load voltage and load current. The load voltage is stable and the harmonic content is low which can be seen from Fig. 22(b). Therefore, the system can provide a high quality voltage for the load. Figure 23(a) and Fig. 23(b) show the dynamic response to the load mutation. We can see that the system has good dynamic performance. The conclusion obtained from the experiment verifies the correctness of the scheme.

V. CONCLUSION

This work presents a three-phase to single-phase ac-dc-ac topology based on multi-converter. It can improve the power quality of electrified railways. The flexible control of the inverter supports the ability to remove all the neutral sections. It has its own advantages in traction applications. Three-phase symmetric structure provides thorough elimination for the

negative sequence current. The series-parallel structure at the output side makes it easy for the capacity expansion to apply in the electrified railways. The H-bridge (HB)-based back-to-back converter supports the easy control system and no neutral potential drift problem. The PWM-based converter adopted in rectifier and the independent control of dc voltage in each module result in little dc voltage unbalance. DC current feedforward control enables it to cope with the impact load, such as the train. Based on the analysis above, a simulation system and a small-scale platform are built. They are all compared with the traditional traction power supply system to validate the effectiveness in solving the power quality problems in the electrified railways. In addition, the basic functions and the dynamic performance are also demonstrated. At the same time, comparing the simulation and experiment results, we can see that adding the number of modules can increase the level of output voltage and the capacity of the system. The analysis above indicates that this topology is very suitable for electrified railways.

It should be noted that only the basic functions of the topology are discussed in this paper. As a matter of fact, the topology also has other functions, such as compensating the voltage sag of the traction network on the heavy haul railway. It can also compensate reactive power and harmonics of the traction load. These studies are under way.

REFERENCES

[1] A. Steimel, "Power-electronic grid supply of AC railway systems," in *Proc. 13th Int. Conf. Optim. Elect. Electron. Equip. (OPTIM)*, Brasov, Romania, May 2012, pp. 16–25.

[2] S. M. M. Gazafrudi, A. T. Langerudy, E. F. Fuchs, and K. Al-Haddad, "Power quality issues in railway electrification: A comprehensive perspective," *IEEE Trans. Ind. Electron.*, vol. 62, no. 5, pp. 3081–3090, May 2015.

[3] G. W. Chang, H.-W. Lin, and S.-K. Chen, "Modeling characteristics of harmonic currents generated by high-speed railway traction drive converters," *IEEE Trans. Power Del.*, vol. 19, no. 2, pp. 766–773, Apr. 2004.

[4] C. Heising, R. Bartelt, M. Oettmeier, V. Staudt, and A. Steimel, "Analysis of single-phase 50-kW 16.7-Hz PI-controlled four-quadrant line-side converter under different grid characteristics," *IEEE Trans. Ind. Electron.*, vol. 57, no. 2, pp. 523–531, Feb. 2010.

[5] M. P. Kazmierkowski, M. Jasinski, and G. Wrona, "DSP-based control of grid-connected power converters operating under grid distortions," *IEEE Trans. Ind. Informat.*, vol. 7, no. 2, pp. 204–211, May 2011.

[6] S.-L. Chen, R. J. Li, and P.-H. Hsi, "Traction system unbalance problem-analysis methodologies," *IEEE Trans. Power Del.*, vol. 19, no. 4, pp. 1877–1883, Oct. 2004.

[7] T.-H. Chen, W.-C. Yang, and Y.-F. Hsu, "A systematic approach to evaluate the overall impact of the electric traction demands of a high-speed railroad on a power system," *IEEE Trans. Veh. Technol.*, vol. 47, no. 4, pp. 1378–1384, Nov. 1998.

[8] S. Lokhande, S. Patil, K. Shende, D. Patil, and A. Mulla, "Introduction to FC-TBSR based SVC for voltage regulation and reactive power compensation," in *Proc. IEEE Int. Conf. Power Electron., Drives Energy Syst. (PEDES)*, Trivandrum, India, Dec. 2016, pp. 1–5.

[9] T. Yoshino and N. Kawakami, "Suppression control of DC current component in SVC originated from even-order voltage harmonics," in *Proc. IEEE 8th Int. Power Electron. Motion Control Conf. (IPEMC-ECCE Asia)*, Hefei, China, May 2016, pp. 3831–3836.

[10] E. Kontos, G. Tsolaridis, R. Teodorescu, and P. Bauer, "High order voltage and current harmonic mitigation using the modular multilevel converter STATCOM," *IEEE Access*, vol. 5, pp. 16684–16692, 2017.

[11] M. Ahmadinia and R. Ghazi, "Coordinated control of STATCOM and ULTC to reduce capacity of STATCOM," in *Proc. Iranian Conf. Elect. Eng. (ICEE)*, Mashhad, Iran, May 2018, pp. 1062–1066.

[12] A. Bueno, J. M. Aller, J. A. Restrepo, R. Harley, and T. G. Habetler, "Harmonic and unbalance compensation based on direct power control for electric railway systems," *IEEE Trans. Power Electron.*, vol. 28, no. 12, pp. 5823–5831, Dec. 2013.

[13] K.-M. Kwon, Y.-S. Song, and J. Choi, "6MVA single-phase APF for high speed train line in Korea," in *Proc. 2nd IEEE Conf. Power Eng. Renew. Energy (ICPERE)*, Bali, Indonesia, Dec. 2014, pp. 31–36.

[14] Y. Mochinaga, Y. Hisamizu, M. Takeda, T. Miyashita, and K. Hasuike, "Static power conditioner using GTO converters for AC electric railway," in *Proc. Conf. Rec. Power Convers. Conf.-Yokohama*, Yokohama, Japan, Apr. 1993, pp. 641–646.

[15] A. Luo, C. Wu, J. Shen, Z. Shuai, and F. Ma, "Railway static power conditioners for high-speed train traction power supply systems using three-phase V/V transformers," *IEEE Trans. Power Electron.*, vol. 26, no. 10, pp. 2844–2856, Oct. 2011.

[16] A. Luo, F. Ma, C. Wu, S. Q. Ding, Q.-C. Zhong, and Z. K. Shuai, "A dual-loop control strategy of railway static power regulator under V/V electric traction system," *IEEE Trans. Power Electron.*, vol. 26, no. 7, pp. 2079–2091, Jul. 2011.

[17] D. Zhang, Z. Zhang, W. Wang, and Y. Yang, "Negative sequence current optimizing control based on railway static power conditioner in V/v traction power supply system," *IEEE Trans. Power Electron.*, vol. 31, no. 1, pp. 200–212, Jan. 2016.

[18] Z. Shu, S. Xie, and Q. Li, "Single-phase back-to-back converter for active power balancing, reactive power compensation, and harmonic filtering in traction power system," *IEEE Trans. Power Electron.*, vol. 26, no. 2, pp. 334–343, Feb. 2011.

[19] Z. Shu, S. Xie, K. Lu, Y. Zhao, X. Nan, D. Qiu, F. Zhou, S. Gao, and Q. Li, "Digital detection, control, and distribution system for co-phase traction power supply application," *IEEE Trans. Ind. Electron.*, vol. 60, no. 5, pp. 1831–1839, May 2013.

[20] A. Nabae, I. Takahashi, and H. Akagi, "A new neutral-point-clamped PWM inverter," *IEEE Trans. Ind. Appl.*, vol. IA-17, no. 5, pp. 518–523, Sep. 1981.

[21] H. Wrede and N. Umbricht, "Development of a 413 MW railway power supply converter," in *Proc. 35th Annu. Conf. IEEE Ind. Electron.*, Porto, Portugal, Nov. 2009, pp. 3587–3592.

[22] J. Ranneberg, "Transformerless topologies for future stationary AC-railway power supply," in *Proc. Eur. Conf. Power Electron. Appl.*, Aalborg, Denmark, Sep. 2007, pp. 1–11.

[23] X. He, Z. Shu, X. Peng, Q. Zhou, Y. Zhou, Q. Zhou, and S. Gao, "Advanced cophase traction power supply system based on three-phase to single-phase converter," *IEEE Trans. Power Electron.*, vol. 29, no. 10, pp. 5323–5333, Oct. 2014.

[24] X. He, A. Guo, X. Peng, Y. Zhou, Z. Shi, and Z. Shu, "A traction three-phase to single-phase cascade converter substation in an advanced traction power supply system," *Energies*, vol. 8, no. 9, pp. 9915–9929, Sep. 2015.

[25] T. Shimizu, K. Kunomura, M. Kai, M. Onishi, H. Masuzawa, H. Miyajima, M. Otsuki, and Y. Tsuruma, "The application of electronic frequency converter to the Shinkansen railyard power supply," in *Proc. Int. Power Electron. Conf. (IPEC-Hiroshima-ECCE ASIA)*, May 2014, pp. 1054–1061.

[26] K. Kunomura, M. Onishi, M. Kai, N. Iio, M. Otsuki, Y. Tsuruma, and N. Nakajima, "Electronic frequency converter feeding single-phase circuit and controlling feeder voltage with fixed power factor method for shinkansen," *IEEE Trans. Power Electron.*, vol. 27, no. 9, pp. 3888–3896, Sep. 2012.

[27] M. Winkelnkemper, A. Korn, and P. Steimer, "A modular direct converter for transformerless rail interties," in *Proc. IEEE Int. Symp. Ind. Electron.*, Bari, Italy, Jul. 2010, pp. 562–567.

[28] T. Schrader, C. Heising, V. Staudt, and A. Steimel, "Multivariable control of MMC-based Static converters for railway applications," in *Proc. Elect. Syst. Aircr., Railway Ship Propuls.*, Bologna, Italy, Oct. 2012, pp. 1–6.

[29] P. Dong, J. Lyu, and X. Cai, "Optimized design and control for hybrid MMC with reduced capacitance requirements," *IEEE Access*, vol. 6, pp. 51069–51083, 2018.

[30] Q. Tu, Z. Xu, and L. Xu, "Reduced switching-frequency modulation and circulating current suppression for modular multilevel converters," *IEEE Trans. Power Del.*, vol. 26, no. 3, pp. 2009–2017, Jul. 2011.

[31] M. Hagiwara, R. Maeda, and H. Akagi, "Control and analysis of the modular multilevel cascade converter based on double-star chopper-cells (MMCC-DSCC)," *IEEE Trans. Power Electron.*, vol. 26, no. 6, pp. 1649–1658, Jun. 2011.

[32] Z. Li, P. Wang, Z. Chu, H. Zhu, Y. Luo, and Y. Li, "An inner current suppressing method for modular multilevel converters," *IEEE Trans. Power Electron.*, vol. 28, no. 11, pp. 4873–4879, Jan. 2013.
[33] Z. Zhang, J. Kuang, X. Wang, and B. T. Ooi, "Force commutated HVDC and SVC based on phase-shifted multi-converter modules," *IEEE Trans. Power Del.*, vol. 8, no. 2, pp. 712–718, Apr. 1993.

LINWEI LI was born in Henan, China, in 1986. He received the B.Sc. and M.Sc. degrees in electrical engineering from Henan Polytechnic University, Jiaozuo, China, in 2011 and 2015, respectively. He is currently pursuing the Ph.D. degree in electrical engineering with Beijing Jiaotong University. His research interests include the theory and technology for traction power supply systems, and electric power quality.

MINGLI WU was born in Hebei, China, in 1971. He received the B.S. and M.S. degrees in electrical engineering from Southwest Jiaotong University, Chengdu, China, in 1993 and 1996, respectively, and the Ph.D. degree in electrical engineering from Beijing Jiaotong University, Beijing, China, in 2006, where he has been a Professor with the School of Electrical Engineering, since 2008. His current research interests include power supplies for electric railways, digital simulation of power systems, and electric power quality.

SI WU was born in Hebei, China, in 1992. She received the B.S. degree in electrical engineering from Beijing Jiaotong University, Beijing, China, in 2015, where she is currently pursuing the Ph.D. degree. Her research interests include control algorithms and pulse-width-modulation (PWM) techniques of multilevel converter for traction power supply systems.

JING LI was born in Henan, China, in 1989. She received the B.Sc. degree in electrical engineering from the North China University of Water Resources and Electric Power, Zhengzhou, China, in 2013, and the M.Sc. degree from Beijing Jiaotong University, Beijing, China, in 2016, where she is currently pursuing the Ph.D. degree in electrical engineering. Her research interests include power quality of electric railways and power electronics in power supply systems.

KEJIAN SONG was born in Hunan, China, in 1988. He received the B.Sc. degree in electrical engineering from Shaoyang University, Shaoyang, China, in 2010, and the M.Sc. degree in electrical engineering from Beijing Jiaotong University (BJTU), Beijing, China in 2012, where he is currently pursuing the Ph.D. degree in electrical engineering.

From December 2014 to December 2015, he was with the Australia Energy Research Institute, UNSW Sydney, Australia, as an Exchange Ph.D. Student, sponsored by the China Scholarship Council. His research interests include modulation methods and control strategies for traction converters and electric power quality of traction power supply systems.